JOURNAL OF Materials CHEMISTRY

Sol–gel synthesis and characterization of Ag_2S nanocrystallites in silica thin film glasses

Lidia Armelao,*[a] Paolo Colombo,[b] Monica Fabrizio,[c] Silvia Gross[d] and Eugenio Tondello[d]

[a]*CNR, CSSRCC, via Marzolo, 1 Padova, Italy. E-mail: armelao@chim02.chin.unipd.it*
[b]*Dipartimento di Chimica Applicata e Scienza dei Materiali, Università di Bologna, viale Risorgimento, 2 Bologna, Italy*
[c]*CNR, IPELP, Corso Stati Uniti, 4 Padova, Italy*
[d]*Dipartimento di Chimica Inorganica, Metallorganica ed Analitica, Università di Padova, via Loredan, 4 Padova, Italy*

Received 28th April 1999, Accepted 11th August 1999

Silver sulfide particles embedded in thin coatings of transparent and homogeneous silica glass are promising materials for the development of optical devices. The optical properties are strongly dependent on the elemental composition and morphology of the coatings as well as on the size distribution of the nanoclusters. A sol–gel route has been used to achieve good control over film composition and morphology. The dip-coating procedure from alcoholic solutions containing tetraethoxysilane [$Si(OEt)_4$] and silver diethylthiourea complexes $[Ag(EtNHCSNHEt)_n]^+$ has been adopted. The silver sulfide particles were directly generated in silica by decomposition of the silver complexes upon heating the coatings. Annealing was performed in a nitrogen atmosphere in order to prevent sulfide oxidation to sulfate. The sol–gel method has been shown to be a suitable procedure for controlling the size of the metal sulfide particles. Evolution of the system under heating has been studied by X-ray photoelectron spectroscopy (XPS), X-ray diffraction (XRD), secondary-ion mass spectrometry (SIMS) and atomic force microscopy (AFM).

Introduction

Insulator glasses doped with nanosized semiconductor crystals, metal oxides or sulfides, have recently attracted much attention for the development of optical devices with controllable linear and non-linear optical properties. Nanoclusters represent an intermediate state of matter between discrete molecules and extended-network solids and their properties, owing to quantum confinement effects,[1–5] are widely diversified as a function of particle size and geometry.[6] Doping of glasses with semiconductor materials has been performed by various methods such as sputtering,[7] ion implantation,[8,9] chemical bath deposition[10] and others. In particular, oxides and sulfide crystals in silica have been obtained mainly by inclusion of pre-formed colloids in a matrix during the gelation process or by ion implantation.[11,12] In the former method, the prepared films can contain undesirable large particles owing to uncontrolled growth and agglomeration processes in the colloidal solution, while in the latter method the outermost layers of the film may be strongly damaged by implantation.

Among synthetic methods, the sol–gel route has gained great practical interest during the last few years for the preparation of advanced materials and in particular to obtain oxide-based coatings.[13] Hydrolysis and condensation reactions lead to the formation of oxo-based macromolecular networks giving scope to tailoring the precursor compounds according to the desired process path. This factor, together with the mild conditions of synthesis ('soft chemistry'), makes the sol–gel method particularly suitable for fabrication of thin films with good control over composition and microstructure. Such films can be doped with molecules or ions and can also contain small aggregates; in addition, the system may be prepared with a homogeneous or heterogeneous distribution of species. Many sol–gel studies described in the literature as synthetic methods for transition metal sulfides have been addressed to embedding pre-formed clusters in a silica matrix, as reported for lead sulfide and cadmium sulfide.[14] In turn, binary metal sulfides have been prepared by direct reaction of the elements at high temperatures for prolonged times, by treatment of element oxides with H_2S or by precipitation of metal cations from aqueous solution upon adding a source of S^{2-}. More recently, a convenient one-step room-temperature preparation of both crystalline and amorphous metal sulfides and selenides at room temperature *via* elemental reactions in liquid ammonia has been described.[15]

This paper reports results for the sol–gel synthesis of Ag_2S-nanoclusters doped silica coatings. Ag_2S is a semiconductor compound and owing to its intrinsic properties, narrow band gap, good chemical stability and ready preparation, it has already been used for the manufacture of optical and electronic devices, such as photovoltaic cells, photoconductors and IR detectors.[16,17] Furthermore, this compound has been used to develop superionic conductors.[18] Moreover, while sulfides like CdS, whose larger band gap ranges between 2.4 and 3.0 eV depending on particle size,[19,20] have been extensively used as window layers, Ag_2S, with an optical band gap of 0.9–1.1 eV,[9,21] may be used as an adsorber layer in thin film solar cells. Silver sulfide is known to exist in three allotropic modifications, each characterised by different chemical–physical properties. α-Ag_2S, known as *achantite*, is monoclinic and thermodynamically stable up to 178 °C.[22,23] At this temperature a reversible order–disorder transition involving an ion conductivity change due to silver sublattice melting occurs.[24] The transformation from *achantite* into the β allotropic form, *argentite*, of bcc structure, occurs through the formation of an intermediate tetragonal phase.[23,25] Above 600 °C the cubic γ phase with fcc structure, of Ag_2S is formed,[23] which melts at *ca.* 825 °C.[26] In this study, the *as prepared* samples contain only silver thiourea complexes which evolve to silver sulfide particles upon heating during densification of the glassy host matrix. In this way, the growth and size of the clusters can be controlled.

The chemical composition of the films was determined by SIMS and XPS, while their microstructure and surface morphology was studied by XRD and AFM, respectively.

Further information has been obtained by UV–VIS spectroscopy.

Experimental

Precursor solutions

Attention was first focused on the synthesis of compounds containing Ag–S bonds for use as precursors for silver sulfide clusters. AgO_2CMe was employed as the silver salt, taking into account that, upon heating, acetate decomposes more readily than other inorganic anions such as nitrate, without leaving residual contaminants inside the coatings. Various organic compounds have been tested as sulfide ion sources: thioacetamide ($MeCSNH_2$), dimethyl sulfoxide (DMSO, Me_2SO) and 1,3-diethyl-2-thiourea (EtNHCSNHEt). Thioacetamide and thiourea are well known sulfur donor compounds and both give complexes with Ag^+ [27] while DMSO has been tested for its basicity towards Lewis acids such as metal ions.[28] Also silver diethyldithiocarbamate [Et_2NCS_2Ag] has been examined as an Ag_2S precursor, since it shows an Ag–S interaction.

Initially, thioacetamide was used. When soluble Ag^+ salts are added to alkaline, neutral or weakly acid aqueous thioacetamide solutions, Ag_2S is formed, whereas in more acidic environments stable complexes $[Ag(C_2H_5NS)_n]^+$ ($1 \leqslant n \leqslant 4$) are observed.[27] A similar behaviour occurs in alcoholic solvents, commonly used in the sol–gel process, but precipitation of Ag_2S is expected at higher pH values. In the adopted sol–gel experimental conditions, which involved the use of weakly acid ethanolic solutions, thioacetamide led to rapid and uncontrolled precipitation of Ag_2S so that use of this reagent was not studied further.

Attempts using DMSO also failed since the mutual solubility of DMSO, silver acetate and ethanol was too low for practical applications.

For silver diethyldithiocarbamate, ebullioscopic and cryoscopic molecular weight measurements, as well as complexing behaviour studies, have shown that in aqueous solution, oligomers of general formula $[Ag(dtc)]_n$ ($n = 5$ or 6) are present.[29,30] Unfortunately, such an oligomerization degree results in a substantial reduction of the solubility of the silver complex in alcoholic solvents.

Consequently, attention was focused on thiourea.[27] In this case, depending on pH and thiourea : silver ratio,[9,27] various complexes $[Ag(thio)_n]^+$ ($n = 1$–4) are formed in solution. A detailed study of all the various species in the Ag^+–thiourea system has been reported in literature.[9,27] In neutral or alkaline environments Ag_2S is formed according to eqn. (1)–(3):[27]

$$Ag{-}S{-}C(NH_2){=}NH_2{}^+ \rightarrow Ag{-}S{-}C(NH_2){=}NH + H^+ \quad (1)$$

$$Ag{-}S{-}C(NH_2){=}NH + Ag^+ \rightarrow Ag_2S + N{\equiv}C{-}NH_2 + H^+ \quad (2)$$

$$2Ag{-}S{-}C(NH_2){=}NH \rightarrow Ag_2S + (NH_2)_2C{=}S + N{\equiv}C{-}NH_2 \quad (3)$$

This reaction runs autocatalytically at $pH > 6.5$, but does not take place under more acidic conditions.[27] In the adopted experimental conditions, *i.e.* at high thiourea concentrations, the complex $[Ag(thio)_4]^+$ is the prevailing species in solution. Once it was established that thiourea was the best compound as a sulfur source, a colourless, transparent and stable solution (A) of the silver sulfide precursor was obtained by dissolving silver acetate and 1,3-diethyl-2-thiourea in anhydrous ethanol in the molar ratio silver acetate : thiourea : ethanol = 1 : 11 : 14. Acetic acid ($MeCO_2H$) was then added to this solution up to an ethanol : acetic acid molar ratio of 1 : 12. A second clear, transparent and stable solution (B) was prepared by dissolving tetraethoxysilane (TEOS) [$Si(OEt)_4$] in ethanol with a TEOS : ethanol molar ratio of 1 : 20. This solution, upon stirring for 1 h at room temperature, was partially hydrolysed upon adding water and acetic acid in a molar ratio silver acetate : acetic acid : water = 1 : 0.14 : 4.9. Then the solution was aged at 60 °C for 10 min. Solutions A and B were then mixed together in the weight ratio of 1 : 1.5 and stirred for some minutes at room temperature before use.

Film deposition

Films were obtained by the dip-coating procedure. Herasil silica slides, $15 \times 25 \times 1$ mm, supplied by Hereaus, were used as substrates. Before use, the slides were cleaned and rinsed both in doubly distilled water and propan-2-ol. This procedure, repeated several times, aimed to remove organic residues at the surface and so favour adhesion between the coating and substrate.[31] The slides were finally dried in air at room temperature. Film deposition was carried out in air with a withdrawal speed of 10 cm min^{-1}. The films were annealed at temperatures ranging between 200 and 600 °C for 1 h.

Thin film characterization

Compositions of films at the surface and in the bulk were investigated by XPS. XPS spectra were run on a Perkin-Elmer Φ 5600ci spectrometer using non-monochromatized Mg-Kα radiation (1253.6 eV) at a working pressure of $< 5 \times 10^{-8}$ Pa. The spectrometer was calibrated assuming a binding energy (E_b) of the Au $4f_{7/2}$ line of 83.9 eV with respect to the Fermi level. The standard deviation for the E_b values was 0.15 eV. The reported E_b values were corrected for charging effects, assigning to the C 1s line of adventitious carbon an E_b value of 285.0 eV.[32] Survey scans were obtained in the range 0–1100 eV. Detailed scans were recorded for the O 1s, Si 2p, Ag 3d, S 2s, S 2p, Ag MNN and S KLL regions. Atomic compositions were evaluated using sensitivity factors supplied by Perkin–Elmer.[33] Depth profiles were carried out by Ar^+ sputtering at 1.5 keV with an argon partial pressure of 5×10^{-6} Pa. The silver oxidation states were evaluated by using the Auger α_1 and α_2 parameters, defined as the sum of E_b for the Ag $3d_{5/2}$ XPS region and the kinetic energies of the Ag M_5NN and the Ag M_4NN Auger peaks, respectively.[34]

XRD measurements were performed using a Philips PW 1820 diffractometer (Cu-Kα radiation, 40 kV, 50 mA) equipped with a thin film attachment (glancing angle = 0.5°). Selected angular ranges were step-scanned several times until a satisfactory signal-to-noise ratio was reached. The instrumental function was determined using an α-SiO_2 sample free from crystal size effects and lattice disorder. For microstructural characterization, an improved profile fitting method[35] using a pseudo-Voigt representation for the line profiles was used. The average crystallite size was calculated using the Scherrer equation, taking into account the instrumental broadening.

SIMS analyses were carried out in a custom-built instrument described elsewhere[36] and recently updated. A monochromatic (2 keV, ionic current range between 400 and 800 nA) $O_2{}^+$ ion beam collimated to 50 μm was generated in a mass-filtered duoplasmatron ion gun (model DP50B, VG Fisons, UK) and a secondary electron multiplier (90° off-axis) was used for negative- and positive-ion detection in counting mode. Lens potentials, quadrupole electronic control units and the detection system were controlled *via* a Hiden HAL IV interface. Surface characterization was carried out by recording mass spectra of both negative and positive ions at different points of the coatings, in order to check composition homogeneity. Signals were attributed to related species by comparing intensity ratios to isotopic patterns, and partial overlapping of ion clusters has been verified by isotopic pattern simulation software.[37] This allowed the confidence interval and residual standard deviations to be calculated for detected ion groups, in order to discriminate between different contributions. Subsequently, upon following signals of interest as a function of

bombarding time, the ion species distribution was studied from the surface to the film/substrate interface.

AFM images were taken using a Park Autoprobe CP instrument operating in contact mode in air. The micrographs were recorded in different areas of each sample, in order to test the film homogeneity. The background was subtracted from the images using ProScan 1.3 software from Park Scientific.

Optical absorption spectra of the systems were recorded in the range 200–1000 nm using a double-beam CARY 5E UV–VIS spectrophotometer with a spectral bandwidth of 1 nm; the contribution from the silica substrate was subtracted.

Results and discussion

The main purpose of this study was to synthesize silver sulfide nanocrystallites embedded into silica layers, with a strict control over cluster size distribution as well as on the purity of the host glassy matrix. To achieve this aim, after deposition at room temperature, the coatings were thermally treated in a temperature range (200–600 °C) suitable to obtain the required purity and also to investigate the compositional and microstructural evolution of the nanoclusters. Annealing was performed in a nitrogen atmosphere to avoid oxidation of sulfide to sulfate. In the presence of oxygen, the formation of silver sulfate is favoured, as suggested by thermodynamic data:[38]

$$\begin{aligned} &Ag_2S_{(s)} + 2O_{2(g)} \rightarrow Ag_2SO_{4(s)} \\ &\Delta G^{\circ}(298\ K) = -702\ kJ\ mol^{-1} \end{aligned} \quad (4)$$

Investigations were first carried out on the 200 °C heat-treated sample. After annealing the coating appeared homogeneous, and was brown-coloured and transparent. The E_b value of the Si 2p line, centred at 103.6 eV, and the corresponding silicon α parameter (1712.2 eV) were in accord with those of silica.[39] However, the O : Si ratio, which was in the range 2.3–2.9 : 1 was greater than that expected for SiO_2, suggesting the presence of residual –OH groups. The E_b values for S 2s (226.3 eV) and S 2p (162.3 eV) regions, typical for S^{2-} containing species, and the silver α parameters ($\alpha_1 = 719.7$ eV, $\alpha_2 = 724.9$ eV) closely matched literature values[33,39] for silver sulfide. However, the presence of the N 1s peak at a position typical for thiourea (400.6 eV), confirmed incomplete degradation of the organic precursor. The presence of thiourea was further supported upon deconvolution of the C 1s signal. Besides adventitious hydrocarbon (284.8 eV) and alkoxy(RC^+H_2OH) (286.1 eV) components, a contribution due to 1,3 diethyl-2-thiourea ($RNHC^+SRNH$) (287.8 eV) was observed. These findings were also corroborated by UV–VIS absorption spectra (Fig. 1). A partial decomposition of the organic precursor could be postulated on the basis of the observed bimodal absorption ($\lambda = 210$ and 242 nm), typical for thiourea.[40] The first absorption is attributed to the $^1n_s \rightarrow {}^1\pi^*$ transition, whereas the second is associated to the transition $^1\pi \rightarrow {}^1\pi$.[41] Consequently, thermal treatment at 200 °C was insufficient to yield pure silica coatings. Moreover, at this temperature, XRD analysis did not reveal the presence of crystalline silver sulfide particles. Taking into consideration all these experimental findings, only the presence of Ag–S bonds could be safely assumed.

After treatment at 300 °C, the samples appeared homogeneous at first glance and were dark grey, in accord with previously reported data for silver sulfide films prepared by chemical bath deposition onto glass substrates.[21] In order to evaluate the stoichiometry and composition of the samples, XPS depth profiles were performed. At and beneath the surface, the E_b values of the Si 2p and O 1s peaks are typical for a silica network, even if an over-stoichiometric O : Si ratio still suggests that the polymerization processes have not yet been completed. For silver, α_1 ranged between 719.0 and 719.6 eV, whereas α_2 lay between 725.3 and 725.9 eV. Both these values are very close to literature data reported for Ag_2S ($\alpha_1 = 719.3$ eV,[39] $\alpha_2 = 724.8$ eV[42] or 725.3 eV[39]). In addition, the S 2p E_b values, lying in the range 161.2–162.6 eV, are in accord with those reported for sulfides (161.0 eV,[39] 162.0 eV[33]) rather than for elemental sulfur (164 eV[33,43]) or sulfates (168.6 eV[43]). In addition, also the observed S 2s E_b values, which ranged between 224.9 and 226.9 eV, are characteristic of sulfide species[43] rather than elemental sulfur (228.0 eV[33]). Finally, Ag 3d and S 2p regions show the same distribution profile throughout the film (Fig. 2), indicating chemical interaction between Ag^+ and S^{2-} species. The presence of unreacted thiourea and silver acetate can be excluded since the C 1s line, at and beneath the surface, shows E_b values typical for hydrocarbon residuals.

In order to confirm the presence of S-containing ionic species, the isotopic pattern of S was monitored on both positive and negative SIMS ion spectra with $m/z = 16$ ($^{16}O^-$), 32 ($^{16}O_2^-$, $^{32}S^-$) and 34 ($^{34}S^-$) ionic signals being followed as a function of the bombarding time. This procedure allowed discrimination of the contributions of both O and S to the ionic yield, revealing the different behaviour of O- and S-related signals, mainly in the deeper regions of the deposits. Analogously, the presence of several Ag_xS^+ ($1 \leqslant x \leqslant 3$) ionic clusters in the silica matrix was observed by analysis of the SIMS spectra (Fig. 3) in terms of isotopic patterns, and by following suitable signals, the related depth profiles have been obtained. In particular it was observed that $m/z = 32$ ($^{32}S^+$), $m/z = 107$ ($^{107}Ag^+$) ion depth profiles (Fig. 4) were substantially invariant. In addition, also the depth profiles (not reported) of the signals at $m/z = 248$ and 355, corresponding to the ion fragments Ag_2S^+ and Ag_3S^+, respectively, showed a similar behaviour indicating the common chemical origin of sulfur and silver. It is also of note that there is a strong analogy with the corresponding XPS depth profiles for sulfur and silver.

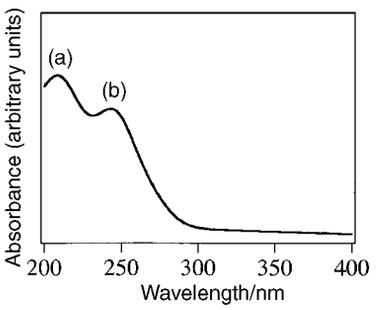

Fig. 1 UV absorption spectrum of the 200 °C annealed sample. The absorption band maxima in (a) and (b) correspond to 210 and 242 nm, respectively.

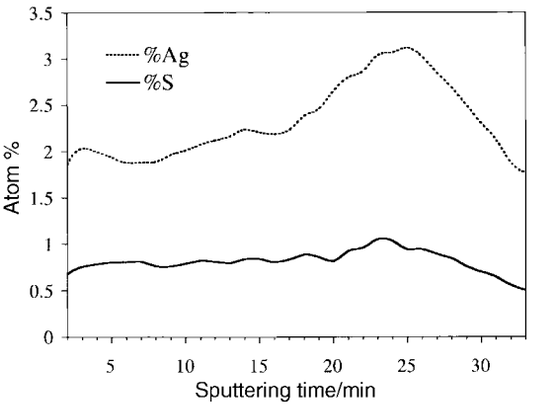

Fig. 2 XPS depth profiles of silver and sulfur for the 300 °C annealed sample.

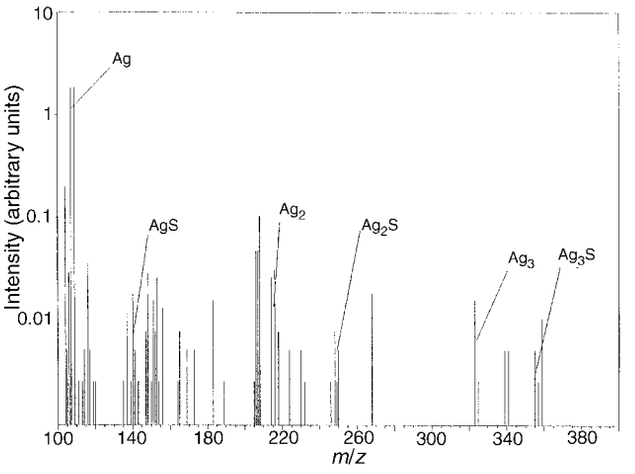

Fig. 3 Positive-ion SIMS spectrum of the 300 °C annealed sample in the range *m/z* 100–400.

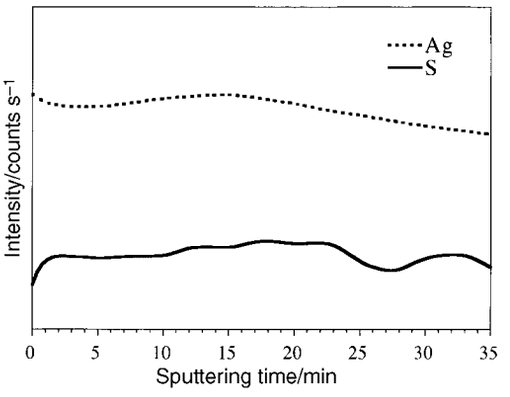

Fig. 4 Positive-ion SIMS depth profiles of silver and sulfur for the 300 °C annealed sample.

Upon thermal annealing at 450 °C, XPS analysis again confirms the presence of silver sulfide throughout the coating. The silver α parameters clearly indicate the formation of silver sulfide ($\alpha_1 = 719.2$–719.7 eV; $\alpha_2 = 724.6$–725.2 eV). This conclusion is also supported by sulfur binding energy values. S 2p E_b values lie in the range 160.3–162.1 eV, *i.e.* at values considerably lower than those typical for elemental sulfur. An analogous behaviour is shown for the S 2s region in the range 224.5–226.1 eV. Finally, the Ag : S ratio is close to the stoichiometric value of 2. SIMS analysis again confirms the presence of Ag_xS^+ species as expected from fragmentation of silver sulfide clusters. In particular, mass spectra show ionic species originating from different isotopic patterns at $m/z = 139$ and 141 (AgS^+), $m/z = 246$, 248 and 250 (Ag_2S^+) and $m/z = 353$, 355, 357 and 359 (Ag_3S^+).

In comparison to the sample annealed at 300 °C, a remarkable depletion of organic fragments is observed, confirming the effectiveness of thermal annealing in improving the film purity, also in agreement with XPS data.

After annealing at 600 °C, XPS analysis suggests a strong variation in the sample chemical composition. In particular, a partial decomposition of Ag_2S to elemental sulfur (S 2p $E_b = 162.1$–163.9 eV, S 2s $E_b = 226.2$–227.7 eV) and metallic silver ($\alpha_1 = 720.0$–720.6 eV, $\alpha_2 = 725.4$–726.0 eV[33,39]) is observed. As reported in the literature,[26] the melting point of bulk Ag_2S is at *ca.* 825 °C, however, simple thermodynamic models predict a lowering in the melting point as the surface energy of the solid becomes higher than that of the liquid. This condition is approached at the nanocrystal size domain for which the surface energy becomes an increasing factor in solid state destabilization.[44] This size-dependent effect can also explain the lowering of the decomposition temperature of silver sulfide observed here.

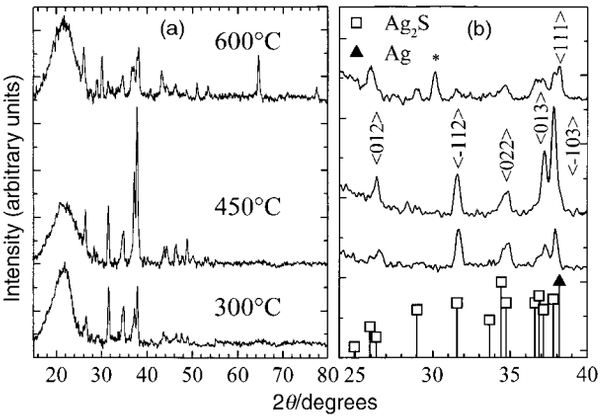

Fig. 5 (a) XRD diffraction patterns for samples heated at 300, 450 and 600 °C. (b) XRD data plotted in a selected angular range, along with the reflections belonging to an Ag_2S and an Ag standard, as reported in the respective JCPDS cards (14–72 for Ag_2S and 4–783 for Ag).

The presence of crystalline silver sulfide clusters has been investigated by XRD. Fig. 5(a) shows diffraction patterns for samples heated at 300, 450 and 600 °C. Fig. 5(b) shows the same data plotted in a selected angular range, along with the reflections for Ag_2S and Ag standards, as reported in the respective JCPDS cards (14–72 for Ag_2S and 4–783 for Ag). The broad band located at 2θ *ca.* 21.5° is due to amorphous silica, present as a host matrix in the films, and as a substrate. Heat treatments at 300 and 450 °C result in the formation of crystalline silver sulfide (α-Ag_2S). The diffraction patterns show that the crystallites are preferentially oriented along the $\langle -103 \rangle$ axis (intense peak located at 37.75°), and the other major peaks are located at 26.35, 31.60, 34.80 and 37.15° (see JPCDS card 14–72).[45] The average crystallite size, computed from the width of three major peaks, lies in the range 25–30 nm for both 300 and 450 °C-treated samples. This rough estimate does not take into account the fact that the anisotropy of the particles may influence the width of the X-ray profile. For the sample heated at 450 °C, the peaks located at 25.92 and 36.84° disappear, and the intensity of those located at 26.35, 37.13 and 37.75° increases. In addition, an intensity increase is observable for the peaks located in the range 2θ 40–50°. This could be attributed either to an increase of the degree of crystallinity in the sample, or to a further orientation of the structure, considering that the intensity of the peaks located at 31.55 and 34.75° seems to be unaltered.

The diffraction pattern for the sample heat treated at 600 °C shows the presence of silver sulfide and metallic silver,[46] in agreement with the XPS findings. In particular, Ag peaks located at 38.12 ($\langle 111 \rangle$), 44.28, 64.43 and 77.48° are clearly visible, and the intensity of the $\langle 220 \rangle$ reflection ($2\theta = 64.43°$) is much higher than that of the standard.[46] There appears to be an alteration in the intensity ratios for the silver sulfide peaks, as well as the appearance of some peaks absent from the patterns for the samples heat-treated at lower temperatures. This suggests that a reduction in orientation of the crystallites is occurring. A peak located at 30.20° [marked by an asterisk in Fig. 5(b)] can be tentatively attributed to silver sulfate (JCPDS card 40–1471); however, XPS data do not indicate the presence of sulfate species in the sample. Since no metallic Ag was observed by XPS in the low temperature-treated samples, we can infer that the development of silver crystallites arises from the decomposition of the silver sulfide clusters. A more detailed investigation is required to clarify the precise mechanism of formation of metallic silver.

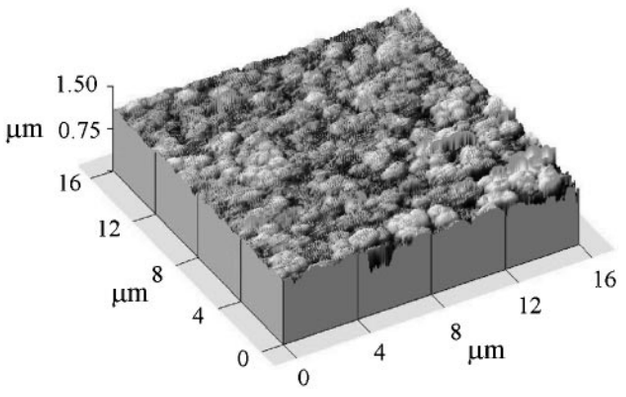

Fig. 6 AFM micrograph of a surface portion (16 μm × 16 μm) for the 300 °C annealed sample.

Finally, concerning the morphology of the coatings, AFM analysis[47] showed a progressive surface flattening after each thermal annealing, as a consequence of densification processes of the host silica matrix. An average roughness[48] of 60 ± 16 nm was estimated for the 300 °C sample (Fig. 6) while after treatment at 450 °C the roughness was reduced to 30 ± 10 nm. In addition, the acquisition of several images taken on different samples areas established the homogeneity of the films surface.

Conclusions

Silver sulfide nanocrystallites have been synthesized directly into a thin silica glassy matrix by a sol–gel process. The choice of suitable organic precursors and low temperature processing has proved to be effective in yielding pure thin films with good cluster size control. The formation and evolution of Ag_2S-silica doped coatings have been studied as a function of thermal annealing performed in a nitrogen atmosphere at a variety of temperatures (200, 300, 450 and 600 °C). The formation of silver sulfide nanocrystals was observed upon heating at 300 °C, as suggested by XRD analysis. The heat treatment results in the formation of crystalline silver sulfide (α-Ag_2S) with an average crystallite size of 25–30 nm. The diffraction patterns show that the crystallites are preferentially oriented along the $\langle -103 \rangle$ axis. XPS and SIMS investigations on the chemical composition of the samples, indicated strong correlation and interactions between silver and sulfur in the films. However, treatment at 300 °C is insufficient to yield a fully polymerized silica matrix. Thermal annealing at higher temperature improved the purity of the host glassy matrix, induced surface flattening and did not affect Ag_2S cluster size. Above 450 °C partial decomposition of silver sulfide to metallic silver and elemental sulfur was observed.

Acknowledgements

This work was partially funded by Progetto Finalizzato 'Materiali Speciali per le Tecnologie Avanzate II' of the CNR (Rome). Thanks are due to Prof. S. Daolio for helpful discussions. The reviewers are gratefully acknowledged for their comments and suggestions.

References

1 J. Warnock and D. D. Awschalom, *Phys. Rev. B*, 1985, **32**, 5529.
2 N. F. Borrelli, D. W. Hall, H. J. Holland and D. W. Smith, *J. Appl. Phys.*, 1987, **61**, 5399.
3 G. Fuxi, *J. Non-Cryst. Solids*, 1991, **129**, 299.
4 L. E. Brus, *J. Chem. Phys.*, 1983, **79**, 5566.
5 S. Schmitt-Rink, D. A. B. Miller and D. S. Chemla, *Phys. Rev. B*, 1987, **35**, 8113.
6 H. Gleiter, *Adv. Mater.*, 1992, **4**, 474.
7 H. Nasu, K. Tsunetomo, Y. Tokumitsu and Y. Osaka, *Jpn. J. Appl. Phys.*, 1989, **28**, L862.
8 C. W. White, J. D. Budai, J. G. Zhu, S. P. Withrow, R. A. Zuhr, Y. Chen, D. H. Hembree Jr., R. H. Magruder and D. O. Henderson, *Mater. Res. Soc. Symp. Proc.*, 1995, **358**, 169.
9 J. G. Zhu, C. W. White, J. D. Budai, S. P. Withrow and Y. Chen, *J. Appl. Phys.*, 1995, **78**, 4386.
10 H. Meherzi-Magharoui, M. Dachraoui, S. Belgacem, K. D. Buhre, R. Kunst, P. Cowache and D. Lincot, *Thin Solid Films*, 1996, **288**, 217.
11 R. Bertoncello, G. Battaglin, F. Caccavale, E. Cattaruzza, P. Colombo, S. Daolio, S. Gross, P. Mazzoldi and F. Trivillin, *J. Mater. Res.*, 1999, **14**, 1.
12 P. Mazzoldi, F. Caccavale, E. Cattaruzza, A. Boscolo-Boscoletto, R. Bertoncello, G. Battaglin and C. Gerardi, *Nucl. Instrum. Methods B*, 1992, **65**, 367.
13 C. J. Brinker and G. W. Scherer, in *Sol–Gel Science: The Physics and Chemistry of Sol–Gel Processing*, Academic Press Inc., San Diego, CA, 1990.
14 M. Guglielmi, A. Martucci, E. Menegazzo, G. C. Righini, S. Pelli, J. Fick and G. Vitrant, *J. Sol–Gel Sci. Technol.*, 1997, **8**, 1017.
15 G. Henshaw, I. P. Parkin and G. Shaw, *Chem. Commun.*, 1996, 1095.
16 R. G. Cope and H. J. Goldsmid, *Br. J. Appl. Phys.*, 1965, **16**, 1501.
17 G. Hodes, J. Manasen and D. Cahen, *Nature (London)*, 1976, **261**, 403.
18 T. Minami, *J. Non-Cryst. Solids*, 1987, **95–96**, 107.
19 N. Tohge, M. Asuka and T. Minami, *J. Non-Cryst. Solids*, 1992, **147–148**, 652.
20 R. D. Stramel, T. Nakamura and J. K. Thomas, *J. Chem. Soc., Faraday Trans. 1*, 1988, **84**, 1287.
21 S. S. Dhumure and C. D. Lokhande, *Thin Solid Films*, 1994, **240**, 1.
22 K. Bozhilov, V. Dimov, A. Panov and H. Haefke, *Thin Solid Films*, 1990, **190**, 129.
23 *Gmelins Handbuch der Anorganischen Chemie*, 61 Ag B3, Verlag Chemie, Weinheim, 1973, pp. 8–56.
24 S. R. Barman, N. Shanthi, A. K. Shukla and D. D. Sarma, *Phys. Rev. B*, 1996, **53**, 3746.
25 A. Boettcher, G. Haase and H. Treupel, *Z. Angew. Phys.*, 1955, **7**, 478.
26 *Handbook of Chemistry and Physics*, ed. R. C. Weast, CRC Press, Boca Raton, FL, 64th edn., 1984, B-137.
27 *Gmelins Handbuch der Anorganischen Chemie*, 61 Ag B7, Verlag Chemie, Weinheim, 1973, pp. 98–136.
28 W. L. Reynolds, *Prog. Inorg. Chem.*, 1970, **12**, 1.
29 A. Tavlaridis and R. Neeb, *Naturwissenschaften*, 1976, **63**, 146.
30 R. Hesse, in *Advances in the Chemistry of the Coordination Compounds*, ed. S. Kirschner, New York, 1961, pp. 314–320.
31 L. Armelao, R. Bertoncello, S. Coronaro and A. Glisenti, *Sci. Technol. Cultural Heritage*, 1998, **7**, 41.
32 M. P. Seah, in *Practical Surface Analysis*, ed. D. Briggs and M. P. Seah, J. Wiley & Sons, New York, 1990, vol. 1, p. 543.
33 J. F. Moulder, W. F. Stickle, P. E. Sobol and K. D. Bomben, in *Handbook of X-Ray Photoelectron Spectroscopy*, ed. J. Chastain, Perkin Elmer Corp., Eden Prairie, MN, 1992.
34 C. D. Wagner, *Anal. Chem.*, 1972, **44**, 972.
35 S. Enzo, S. Polizzi and A. Benedetti, *Z. Kristallogr.*, 1985, **170**, 275.
36 C. Pagura, S. Daolio and B. Facchin, in *Secondary-Ion Mass Spectrometry SIMS VIII*, ed. A. Benninghoven, K. T. F. Jansen, J. Tumpner and H. W. Werner, John Wiley, Chichester, 1992, p. 239.
37 C. Pagura and S. Valcher, unpublished work.
38 O. Knacke, O. Kubaschewski and K. Hesselmann, in *Thermochemical Properties of Inorganic Substances*, Springer Verlag, Berlin, 1991, vol. 1.
39 C. D. Wagner, in *Practical Surface Analysis*, ed. D. Briggs and M. P. Seah, J. Wiley & Sons, New York, 1990, vol. 1, pp. 595–604.
40 J. Barrett and F. S. Deghaidy, *Spectrochim. Acta, Part A*, 1974, **31**, 707.
41 H. Hosaya, J. Tanaka and S. Nagakura, *Bull. Chem. Soc. Jpn.*, 1960, **33**, 850.
42 V. K. Kaushik, *J. Electron Spectrosc. Relat. Phenom.*, 1991, **56**, 273.
43 *XPS Photoelectron Spectroscopy Database*, version 1.0, National Institute of Standards and Technology, Gaithersburg, MD, 1989.
44 A. N. Goldstein, C. M. Echer and A. P. Alivisatos, *Science*, 1992, **256**, 1425.

45 Pattern 14–72 on Joint Committee on Powder Diffraction Standard, International Centre for Diffraction Data, Newton Square, PA, 1992.
46 Pattern 4–783 on Joint Committee on Powder Diffraction Standard, International Centre for Diffraction Data, Newton Square, PA, 1993.
47 K. L. Westra and D. J. Thomson, *Thin Solid Films*, 1995, **257**, 15.
48 *User's Guide to Autoprobe CP and LS*, Park Scientific Instruments, Sunnyvale, CA, 1996.

Paper 9/03377G